Molecular Functions of Conserved Aspects of the GHMP Kinase Family†

John L. Andreassi II and Thomas S. Leyh*

The Department of Biochemistry, Albert Einstein College of Medicine, 1300 Morris Park Avenue, Bronx, New York 10461-1926

Received May 21, 2004; Revised Manuscript Received August 31, 2004

ABSTRACT: The sequences and three-dimensional structures of the galactokinase, homoserine kinase, mevalonate kinase, and phosphomevalonate kinase (GHMP) family were compared to identify highly conserved surface residues. The functions of these solvent-accessible residues were assessed by determining the effects of their substitution, via mutagenesis, on the initial-rate parameters of a representative member of the GHMP kinase family, phosphomevalonate kinase from *Streptococcus pneumoniae*. What emerges from this study is a profile of the conserved surface-linked functions of the family. Certain substitutions produce highly selective effects on the steady-state affinity of a particular substrate, while one residue, Asp150, appears to be a pure k_{cat} effector. Substitutions elsewhere affect multiple initial-rate parameters with varying, and sometimes compensatory, patterns. An α-helix that repositions during catalysis was substituted along its length to assess how its different segments contribute to catalysis—the substrate-proximal edge of the helix affects ATP recognition and k_{cat}, while the distal edge affects recognition of both substrates without affecting turnover. GHMP kinase mutations at the conserved surface residues corresponding to Ser291 and Ala293 in phosphomevalonate kinase are linked to mevalonic acid deficiency, which can lead to early fatality, and galactokinase deficiency, which causes cataracts. Our results suggest that the molecular basis for this particular galactokinase deficiency is an increase in the K_m for galactose.

The (GHMP) kinase superfamily (*1*, *2*) is composed of 581 unique protein sequences, and the Protein Data Bank (PDB)[1] contains the structures of eight different members of the family. Sequence identity among the eight is low (10−20%), yet they share a great deal of three-dimensional similarity (C_α RMSDs range from 2.6 to 4.0 Å). Apparently, the structural scaffold of the family has been maintained, while the residues have been allowed to drift. The result is a family that has evolved to contain nominally seven different catalysts (mevalonate kinase, phosphomevalonate kinase, diphosphomevalonate decarboxylase, archeal shikimate kinase, galactokinase, homoserine kinase, and 4-(cytidine 5′-diphospho)-2-*c*-methyl-D-erythritol kinase), each designed to transfer the γ-phosphoryl group of ATP to a different acceptor, and a nonenzymatic protein, Xol-1, that regulates development in *Caenorhabditis elegans* (*3*). Of the seven enzymes, six kinases and one decarboxylase, two have been linked to human disease (*4*, *5*), two are involved in the biosynthesis of aromatic and nonaromatic amino acids, folates, and ubiquinones (*6*, *7*), one is needed to deliver galactose to the glycolytic pathway (*8*), and four are essential for either the mevalonate- or non-mevalonate-dependent synthesis of isoprenoids (*6*, *9*−*13*), a complex class of metabolites encompassing ∼25 000 compounds including cholesterol, vitamin A, chlorophyll, Taxol, and geranylgeranyl and farnesyl diphosphates (*14*).

The goal of the present study is to identify the highly conserved solvent-accessible residues that are characteristic of the GHMP kinase family, to mutate them to assess their molecular function(s), and to thereby profile the functions of the surface-conserved aspects of the family. In cases where the literature can be brought to bear, the profile extrapolates well across the family, which leads to the hypothesis that one of the causes of cataract formation is a decrease in the steady-state affinity of galactokinase for galactose. Phosphomevalonate kinase (PMK) was chosen as the representative member of the GHMP kinase family for this study because its mechanism is well-defined, its structure has been determined, and its sequence is characteristic of the family.

Phosphomevalonate kinase (ATP−5-phosphomevalonate phosphotransferase, E.C. 2.7.4.2) catalyzes transfer of the γ-phosphoryl group of ATP to (*R*)-5-phosphomevalonate (Pmev), resulting in formation of ADP and (*R*)-5-diphosphomevalonate, DPM (reaction 1). The PMK-catayzed

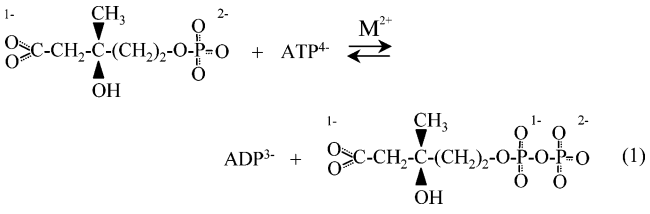

reaction is the second step in the so-called mevalonate pathway, a series of four enzymes the successive actions of which produce isopentenyl diphosphate, the five-carbon building block used for isoprenoid biosynthesis. Phosphoryl-

† Supported by the National Institutes of Health Grant GM54469 and the Albert Einstein College of Medicine.

* Corresponding author. Mailing address: The Department of Biochemistry, Albert Einstein College of Medicine, 1300 Morris Park Ave., Bronx, NY 10461-1926. Phone: 718-430-2857. Fax: 718-430-8565. E-mail: leyh@aecom.yu.edu.

[1] Abbreviations: 2-ME, β-mercaptoethanol; DTT, dithiothreitol; Hepes, *N*-2-hydroxyethylpiperazine-*N*′-2-ethanesulfonic acid; Tris, trishydroxymethyl aminomethane; BLOSUM, blocks substitution matrix; PDB, Protein Data Bank; U, unit (1 μmol of product formed per minute at saturating substrate(s)).

10.1021/bi048963o CCC: $27.50
Published on Web 10/30/2004

transfer between the two phosphate monoester dianions, ADP and Pmev, is essentially isoenergetic (K_{eq} ranges from 1.7 to 7.5 under near-physiological conditions (*9*, *15*)). The *Streptococcus pneumoniae* enzyme is a monomer (37 kDa) in solution; however, the apoenzyme crystallizes as a hexamer (*11*). The kinetic mechanism is random sequential bi-bi in both directions (*9*, *16*).

MATERIALS AND METHODS

Lactate dehydrogenase (LDH, rabbit muscle), pyruvate kinase (PK, rabbit muscle), NADH, phenylmethylsulfonyl fluoride (PMSF), and pepstatin were purchased from Roche Applied Science. ATP, phosphoenolpyruvate (PEP), β-mercaptoethanol (2-ME), dithiothreitol (DTT), reduced glutathione (GSH), and KH_2PO_4 were purchased from Sigma. NaCl, KCl, Hepes, Tris, $MgCl_2$, KOH, glycerol, and Luria−Bertani Miller (LB) media and LB-agar were purchased from Fisher. Isopropyl-1-thio-β-D-galactopyranoside (IPTG) was purchased from Labscientific. Chelating Sepharose Fast Flow and glutathione Sepharose 4 Fast Flow resin and GSTrap columns were aquired from Amersham Biosciences. Competent *Escherichia coli* BL21(DE3) were purchased from Novagen and *E. coli* XL1-Blue competent cells were purchased from Stratagene. Mevalonate kinase from *S. pneumoniae* was expressed in BL21(DE3) cells as an N-terminal GST fusion protein and purified on a GSTrap column to ≥95% homogeneity (*9*). Mevalonate and phosphomevalonate were chemically or enzymatically synthesized as described in ref *9*. A plasmid encoding *Saccharomyces cerevisiae* mevalonate-5-diphosphate decarboxylase (MDD) was used to express an N-terminal 6×-His−MDD fusion protein. Recombinant MDD was expressed in BL21(DE3) cells and purified to ≥95% purity by metal ion (Ni^{2+}) affinity chromatography.

Site-Directed Mutagenesis. Site-directed mutations were introduced using an oligonucleotide-directed strategy following protocols associated with the QuickChange site-directed mutagenesis procedures (Stratagene). The PCR-amplified DNA was treated with *Dpn*I and used to transform competent XL1-blue *E. coli* cells. Plasmids were isolated and sequenced (Albert Einstein College of Medicine DNA sequencing facility) across the region encoding the entire His-GST−PMK fusion protein to verify the introduction of the correct mutation into the PMK cDNA and to ensure that the sequence encoding the fusion protein was free of PCR-generated errors.

Circular Dichroism (CD) Spectra. CD spectra of all PMKs used in this study were collected using a Jasco J-270 spectropolarimeter (cell length = 0.02 cm). The samples contained PMK (4.0 μM), Hepes/K^+ (2 mM, pH 8.0), and KCL (5.0 mM) (*17*). CD data were collected from 200 to 250 nm and converted to molar ellipticity. The CD spectra of the native and mutant PMKs used in this study are virtually identical, suggesting that the secondary structural composition of the mutant and wild-type proteins are similar (*18*).

The PMK Expression Vector. The cDNA of *S. pneumoniae* (R6) was subcloned into a pGEX vector that was modified to express a 9×-histidine peptide fused to the N-terminus of GST (pGEX-His-GST). This dual affinity tag was removed from the PMK fusion protein (~64 kDa) by proteolysis using Precision Protease, which leaves the GPLHM peptide attached at the PMK N-terminus.

Expression and Purification of Wild-type and Mutant PMK Enzymes. PMK wild-type and mutant fusion proteins were purified to homogeneity using immobilized metal-ion affinity chromatography followed by glutathione affinity chromatography (Amersham-Pharmacia product manuals). Freshly transformed BL21(DE3) *E. coli* colonies containing an expression plasmid encoding a His-GST−PMK fusion protein were used to inoculate a 1.0 L LB culture containing 50 mg/L ampicillin. The cells were grown at 37 °C to OD_{600} = 0.8, cooled to 17 °C, and protein expression was induced by the addition of isopropyl-1-thio-β-D-galactopyranoside to a final concentration of 0.7 mM. The culture was then incubated at 17 °C for 17 h, and cells were harvested by centrifugation. The cell pellet (~4 g of cell paste) was suspended in 20 mL of KPO_4 buffer (50 mM, pH = 7.3, 25 °C) containing lysozyme (0.1 mg/mL), PMSF (290 μM), pepstatin A (1.5 μM), KCl (0.4 M), and 2-ME (5 mM). The mixture was stirred for 1 h at 4 °C prior to sonication (Branson Sonifier). Cell debris was removed by centrifugation (45 min, 4 °C, RCF = 34 000 × *g*), and the supernatant was loaded onto a 5 mL Chelating Sepharose Fast Flow column charged with Ni^{2+} and equilibrated with buffer A (KPO_4 (50 mM, pH = 7.3), KCl (0.4 M)). The column was then washed with 10 bed volumes of buffer B (KPO_4 (50 mM, pH = 7.3), imidazole (10 mM), 2-ME (5 mM), and KCl (0.4 M)). The fusion protein was then eluted from the Ni^{2+}-chelated Sepharose column with 10 bed volumes of buffer C (KPO_4 (50 mM, pH = 7.3), imidazole (250 mM), 2-ME (5 mM), and KCl (0.4 M)) directly onto a 5 mL glutathione Sepharose column equilibrated in buffer D (KPO_4 (50 mM, pH = 7.3), DTT (2 mM), and KCL (0.4 M)). The glutathione Sepharose column was then washed with 10 bed volumes of buffer D, and then PMK fusion protein was eluted with 20 mL of buffer E (Tris (100 mM, pH = 8.0), DTT (2 mM), GSH (10 mM), and KCl (0.4 M)). The fusion protein was then digested with Precision Protease in an overnight dialysis against Hepes/K^+ (50 mM, pH = 7.5), DTT (1.5 mM), and KCl (0.05 M) at 4 °C. After dialysis, the sample was passed back through the glutathione column equilibrated in buffer F (Hepes/K^+ (50 mM, pH = 7.5), DTT (2 mM), and KCl (0.05 M)) to remove the His-GST tag and Precision Protease. The flow-through containing PMK was collected, concentrated in an Amicon Ultra centrifugal filter (10 kDa cutoff; Millipore) to approximately 10 mg/mL, and stored at −80 °C in 40% glycerol. The protein preparations, assessed using SDS−PAGE, were >97% pure. Protein concentrations were determined spectrophotometrically by absorbance at 280 nm, $\epsilon_{280} = 42.5\ mM^{-1}\ cm^{-1}$.

Steady-State Kinetics of the Forward PMK Reaction. Kinetic parameters for wild-type and mutant PMKs were determined using a high-throughput progress-curve assay in which the concentration of ATP was held fixed, using a regenerating system, while >98% of the Pmev was consumed. Obtaining initial rates throughout the entire progress curve required that the products, ADP and diphosphomevalonate, be continuously removed by coupling enzymes. Diphosphomevalonate was converted to isopentenyldiphosphate (which did not inhibit PMK) using recombinant diphosphomevalonate decarboxylase (MDD), and the ADP produced by both PMK and MDD reaction was removed

and converted to ATP by the successive actions of pyruvate kinase (PK) and lactate dehydrogenase (LDH). The concentrations of coupling enzymes were such that each reaction reached a steady-state in ≤9 s (*19*). Typical progress-curve reaction conditions are as follows: PMK (26 nM), ATP (5, 1.1, and 0.55 × $K_{m,ATP}$), Pmev (10 × $K_{m,Pmev}$), MDD (0.4 U/mL), PK (5 U/mL), LDH (10 U/mL), PEP (1.0 mM), [$MgCl_2$] = [ATP] + 1 mM, NADH (0.25 mM), Hepes/K^+ (50 mM, pH = 8.0), KCl (50 mM), T = 25 ± 2 °C. The time required for reactions to reach completion ranged from 10 to 20 min. The concentration of phosphomevalonate was determined at each point in the progress curve from the absorbance at 339 nm, and the velocity was calculated from the slope of the line ($(-d[S])/dt$) taken over an interval that was centered on a given point and that spanned 1.5−2% of the overall reaction. Typically, V and [S] pairs were extracted from the 10 000−15 000 data points associated with a single progress curve, and kinetic parameters were obtained by statistically fitting the pairs to a model for a sequential reaction mechanism using the *SEQUEN* program, developed by W. W. Cleland (*20*), that was modified to accept large datasets.

The A293T Mutant. Because the extremely large $K_{m,Pmev}$ of the PMK A293T mutant prevented successful progress-curve studies of this mutant, traditional initial-rate measurements were used to estimate the Michaelis constants for phosphomevalonate and ATP. The activity of the A293T mutant was measured in a spectrophotometric-based assay that coupled the production of ADP to the oxidation of NADH via pyruvate kinase and lactate dehydrogenase. Assay mixtures used to determine $K_{m,Pmev}$ contained PMK A293T (25 μM), phosphomevalonate (0−25 mM, the highest achievable Pmev concentration), ATP (10 mM), Hepes/K^+ (50 mM, pH = 8.5), β-NADH (0.3 mM), PEP (1.0 mM), [$MgCl_2$] = [nucleotide] + 1 mM, pyruvate kinase (2.5 U/mL), lactate dehydrogenase (5 U/mL), and MDD (0.2 U/mL). The $K_{m,ATP}$ was determined under identical conditions described above except that phosphomevalonate was fixed at 20 mM and the ATP substrate was varied from 0 to 10 mM. Data were fit to a rectangular hyperbola using the *HYPERO* algorithm (*20*) to obtain $K_{m,Pmev}$ and $K_{m,ATP}$. It is important to realize that the K_m values are apparent due to the inability to saturate A293T with phosphomevalonate and could be significantly lower.

Inhibition of PMK by Mevalonate. Mevalonate, a dead-end inhibitor of PMK, is competitive against phosphomevalonate and noncompetitive against ATP (*9*). $K_{i,Mev}$ was determined for wild-type and K9R PMK using the Dixon experimental design (*21*). Initial rates were measured at six mevalonate concentrations (0, 125 μM, 250 μM, 500 μM, 1.0 mM, and 2.0 mM) at fixed concentrations of phosphomevalonate ([Pmev] = 4 × $K_{m,Pmev}$) and MgATP ([ATP] = 7 × $K_{m,ATP}$, [$MgCl_2$] = [nucleotide] + 1 mM). The assay conditions were identical to those described in the section entitled Steady-State Kinetics of the Forward PMK Reaction. Kinetic constants were obtained by statistically fitting the data in $1/V$ vs [I] format using Graph Pad. Values for $K_{i,Mev}$ were calculated using the Dixon equation for a competitive inhibitor (*21*): $[I] = -K_i(1 + [S]/K_m)$, where I = negative X-axis intercept, S = Pmev, and $K_m = K_{m,Pmev}$.

RESULTS AND DISCUSSION

Residue Selection. The goal of the selection was to define a set of residues that are representative of the highly conserved solvent-accessible residues found in the GHMP kinase family. These target residues were mutated, and the effects of mutation were studied to obtain descriptions of the molecular functions of the conserved aspects of the family. The approach focuses on residues that have been conserved in the surface layer of the family's architecture—the interface through which these proteins recognize and interact with their environment. Targets were identified in several ways. The primary sequences of the GHMP kinase family were compared to identify both family-wide and PMK-specific conservation. These conserved residues were then mapped onto the PMK structure to assess their surface accessibility. Solvent-accessible residues that are well-conserved in three-dimensional space but not in sequence space were identified by visual inspection of the GHMP kinase structures, which were superposed using the Vector Alignment Search Tool (VAST) (*22*, *23*). These two screens ultimately identified 20 target residues, nine of which appeared to be integral to the structural core of the enzyme and were therefore removed from further consideration. The remaining 11 were mutated; nine of which expressed at detectible levels and were characterized. These nine residues are colored red in the apo-PMK structure shown in Figure 1, panel A.

The GHMP kinase superfamily, as defined by the Protein Families Database (*24*), contains 581 sequences. This evolving set of sequences provides a lower limit for the number of sequence-distinct proteins that this work will impact. Removing hypothetical proteins and protein fragments from the set of 581 left a core set 142 sequences. These 142 sequences were separated into seven groups according to EC number. Alignments were constructed for each group using Clustal W (BLOSUM matrix), and consensus sequences were obtained using BoxShade 3.21, which defines a consensus residue as one that is present in 50% or more of the residues in a Clustal W alignment column (alignments can be viewed in Supporting Information). The consensus residues were mapped onto the sequence of PMK and then onto its structure to assess their solvent accessibility. Surface residues conserved in the atomic architecture of the family but not in the primary sequences were identified by comparing the structures of the eight family members for which structures are available (phosphomevalonate kinase (1K47), mevalonate kinase (1KVK and 1KKH), homoserine kinase (1H72), 4-(cytidine 5′-diphospho)-2*c*-methyl-D-erythritol kinase (1UEK), Xol-1 (1MG7), mevalonate 5-diphosphate decarboxylase (1FI4), and galactokinase (1PIE and 1S4E)). The sequence conservation of the target residues across each EC class, as predicted by ClustalW, is compiled in Table 1. Conservation determined using sequence analysis does not in all cases agree with that determined using structural analysis. Those cases in which conservation predicted by structure- and sequence-based alignments disagree significantly are indicated in Table 1. The residues that are not conserved across multiple classes (Q218, K221, and Q222) were selected on the basis of the conservation of the structural element in which they reside (see A Mobile Active-Site α-Helix, below).

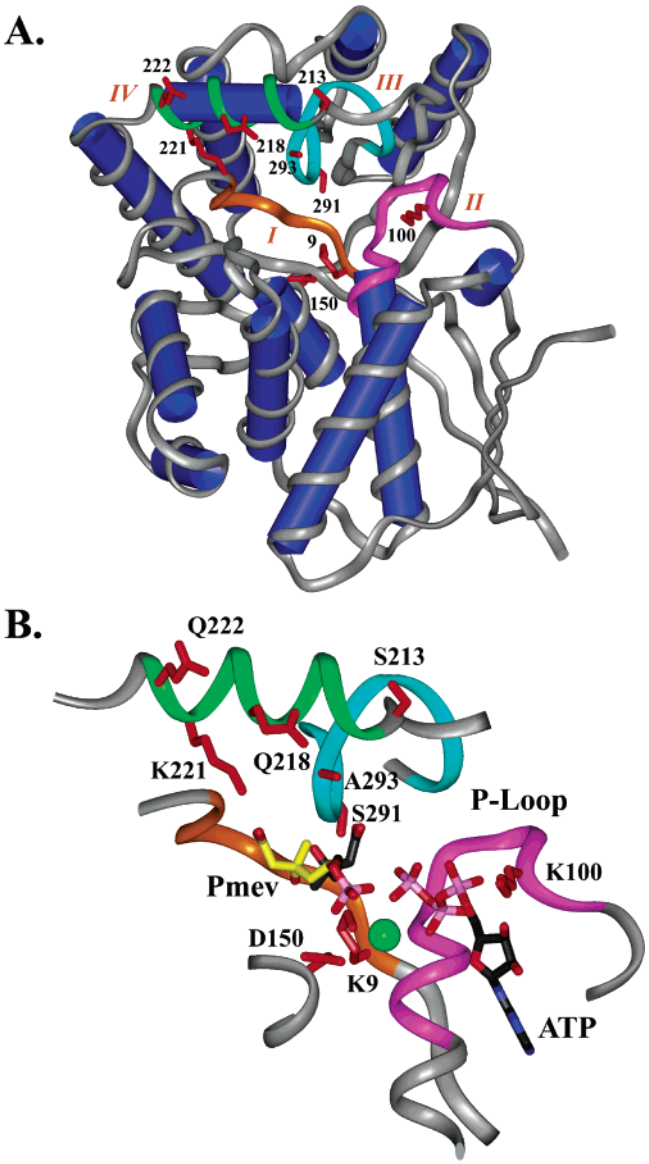

FIGURE 1: Mutagenesis and modeling of the PMK structure. In panel A, the set of surface conserved residues that are the mutagenesis targets in this study are shown in red. The conserved motifs that are characteristic of the GHMP kinase family are colored as follows: motif I (orange); motif II (magenta); motif III (cyan); mobile α-helix (green). Panel B shows modeling of substrates into the Apo-PMK structure. MgATP was positioned as it appears in structure of the rat MVK·MgATP complex. Phosphomevalonate is shown in two possible conformations based on the placement of homoserine in the *M. jannaschii* HSK·AMPPNP·homoserine complex (yellow) and the modeling of mevalonate in the rat MVK·MgATP complex (black). The Pmev 5-phosphate was positioned to react with the γ-phosphate of ATP. To properly dock the substrates, the torsion angles of two active-site side chains were changed: Tyr 11 was rotated 39° about the $C_\beta-C_\gamma$ bond, and Lys9 was rotated 120° about the $C_\delta-C_\epsilon$ bond.

A Structural Model for PMK. The only available PMK structure (*S. pneumoniae*) is devoid of substrates. To better interpret the results reported here, a model of the ternary PMK complex (PMK·phosphomevalonate·MgATP) was constructed from the structures of other GHMP kinase·substrate complexes. ATP was positioned in the active site using the rat mevalonate kinase·MgATP (MVK) structure as a guide—the ATP conformation was not changed, and the nucleotide is positioned identically relative to the backbone of a highly conserved peptide (Gly-Leu-Gly) that forms part of the nucleotide-binding loop (Figure 1, panel B). The position of this loop relative to the nucleotide is virtually indistinguishable in the two GHMP kinase structures in which nucleotide is bound (*10*, *25*).

Two phosphomevalonate conformations, which differ in the position of the carboxylate, were considered in the interpretations (Figure 1, panel B). The first uses the conformation and positioning of homoserine seen in the homoserine kinase·AMPPNP·homoserine (HSK) complex (*10*). Motif III, which is very highly conserved, was used to position homoserine in PMK precisely as it appears in the homoserine kinase E·AMPPNP·homoserine complex. Homoserine was then elaborated into phosphomevalonate, and the 5-phosphate was positioned to react with the γ-phosphate of ATP. The second carboxylate conformation is predicted by the modeling studies used to position mevalonate in the rat MVK active site (*25*).

Initial-Rate Studies Using Progress Curves. The initial-rate mechanism of the *S. pneumoniae* PMK is random sequential in both directions; that is, substrates bind randomly to the active site, which must be occupied simultaneously by both substrates to accomplish phosphoryl transfer (*9*). To rapidly evaluate the initial-rate behavior of wild-type and mutant PMKs, a progress-curve assay was devised (see Materials and Methods). The method offers significant technical advantages over approaches that involve initial-rate measurements at each of a variety of substrate concentrations. In particular, the error in relative substrate concentration, which is monitored continuously in a stationary cuvette, is extremely small, yielding precise data that extends smoothly to the limits of detection of a given instrument. The result of a typical progress-curve experiment, presented in double-reciprocal format, is shown in Figure 2.

Motif I—A Catalytic Lysine. GHMP kinase active sites exhibit a well-conserved seven-residue sequence known as motif I (*11*). Lysine 9, located at the N-terminus of the motif, is a particularly well-conserved element and is positioned in our model to interact with the phosphoryl group of phosphomevalonate. Replacing the ammonium ion of Lys9 with the guanidinium group of arginine causes an ~52-fold increase in both K_i and K_m for Pmev, a 450-fold decrease in k_{cat}, and a slight (1.6-fold) decrease in K_i and K_m for ATP (Table 2). The selective effect of the mutation on the affinity of Pmev supports the structural suggestion that Lys9 interacts with the Pmev phosphoryl moiety during turnover. The fact that K_i/K_m is not affected by the mutation indicates either that Lys9 is not involved in the substrate-driven reorganization of the active site seen in wild-type PMK or that the substrate interactions with this residue in both forms of the enzyme are affected equally. The effect of the mutation on the rate-determining step(s) of the reaction (450-fold) is considerably greater than its influence on the steady-state affinity constants. Given its position and the effects of its substitution on k_{cat}, it is plausible that the role of this highly conserved, positively charged residue is to neutralize the negative charge that develops as phosphoryl-transfer reactions move into the transition state (*26*).

The hypothesis that Lys9 interacts with the 5-phosphate of Pmev was assessed further by determining the effects of Lys9 mutation on the affinity of mevalonate, which lacks the 5-phosphate and is a competitive inhibitor vs Pmev (*9*).

Table 1: Sequence Conservation (%) of PMK Target Residues across the EC Classes Found in the GHMP Kinase Family

target PMK residue	phosphomevalonate kinase EC 2.7.4.2	mevalonate kinase EC 2.7.1.36	homoserine kinase EC 2.7.1.39	galactokinase EC 2.7.1.6	shikimate kinase EC 2.7.1.71	erythritol kinase EC 2.7.1.148	mevalonate diphosphate decarboxylase EC 4.1.1.33
K9	100[a]	100	55[d]	100	86	100	100[d]
K100	66	—[b]	—[b]	—[b]	—[b]	—[b]	—[b]
D150	100	100	—[b]	—[b,d]	—[b]	100	—[b]
S213	100	100	55	—[b]	—[b]	60	100
S291	100	100	100[d]	90	86	100	—[b]
A293	75	54	60[d]	52	—[b]	—[b]	92
Q218[c]	—[b,d]	—[b]	—[b]	—[b]	—[b]	—[b]	—[b,d]
K221[c]	—[b,d]	—[b]	—[b]	—[b,d]	—[b]	—[b,d]	—[b]
Q222[c]	—[b]	—[b]	—[b]	—[b]	—[b]	—[b]	—[b]

[a] The percentage of ClustalW-aligned sequences within an EC class that are conserved when compared to the target PMK residue. [b] No significant conservation detected. [c] Residue selected on the basis of position in an α-helix that is highly conserved across the family. [d] Indicates a significant discrepancy between conservation predicted by sequence- and structure-based alignments.

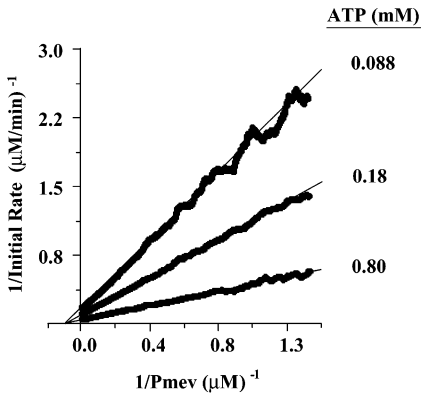

FIGURE 2: A representative double-reciprocal progress-curve study—the K221R mutant. To prevent product inhibition, both of the products of the reaction, ADP and diphosphomevalonate, were continuously removed. ADP was converted into ATP (the concentration of which remained fixed throughout the reaction) using pyruvate kinase, and diphosphomevalonate was converted to isopentenyl diphosphate, which did not detectibly inhibit PMK or the coupling enzymes under the conditions used. The assay conditions were as follows: PMK (26 nM), ATP (5.0, 1.1, and $0.55 \times K_{m,ATP}$), Pmev ($10 \times K_{m,Pmev}$), MDD (0.40 U/mL), PK (5.0 U/mL), LDH (10 U/mL), PEP (1.0 mM), $[MgCl_2] = [ATP] + 1.0$ mM, NADH (0.25 mM), Hepes/K^+ (50 mM, pH = 8.0), KCl (50 mM), $T = 25 \pm 2$ °C. Initial rates were computed from the slopes of the progress curves taken over intervals ranging from 1% to 1.5% of total reaction. Slopes were computed at 10 000−20 000 evenly spaced points between 5% and 95% of reaction. The initial-rate parameters were obtained by statistically fitting the $1/V$ vs $1/S$ data to a sequential bi-bi model using *SEQUEN*, which was modified to accept larger datasets (see Materials and Methods).

A classical initial-rate inhibition study was used to assess the effects of mutation on the inhibition constant of mevalonate. The protocol for this inhibition study is described in Materials and Methods, and the results are compiled in Table 3. The K9R mutation increases $K_{m,Pmev}$ 54-fold but has little, if any, effect on $K_{i,Mev}$. Loss of the phosphoryl-group reduces the effect of the mutation on ligand affinity to near-zero, which supports direct interactions between the residue and the group.

A previous study using a different member of the GHMP kinase family, rat mevalonate kinase, replaced the motif I lysine with a methionine (*27*). The initial-rate effects of this replacement, although different in magnitude, exhibited the same pattern seen in the current study (56-fold decrease in k_{cat}, 10-fold increase in $K_{m,Mev}$, and a 7-fold decrease in $K_{m,ATP}$) suggesting that the molecular function(s) of at least certain of the conserved surface residues extrapolate across members of the GHMP kinase family.

Motif II—The P-Loop. GHMP kinases contain a P-loop that is structurally distinct from the prototypical Walker P-loop (*2*, *28*). The Mg^{2+}-nucleotide conformations differ significantly, as do the ways in which the nucleotides dock into their respective loops. Lysine 100 is situated at the N-terminal end of the P-loop, and its ammonium group is oriented such that it seems likely to interact with ATP (N_ζ is ∼2.6 Å from the 3′-hydroxyl and ∼3.3 Å from the oxygen that bridges the α-phosphate and 5′-carbon). Removing the ammonium ion, by substitution with alanine, caused an ∼10-fold increase in both the K_m and K_i for ATP and small effects (1.7−3-fold) on $K_{i,Pmev}$, $K_{m,Pmev}$, and k_{cat}. The more conservative replacement of Lys100 with an arginine results in a slight (2-fold) restoration of the steady-state affinity of the enzyme for ATP and, interestingly, increases k_{cat} 3-fold over the wild-type enzyme. These data confirm that Lys100 impacts the stability of the $E{\cdot}Mg^{2+}$−ATP complexes during steady-state turnover and are consistent with a direct interaction with ATP.

The remaining P-loop residues that were selected for mutagenesis, Ser106 and Ser107, did not express at detectable levels in *E. coli*. However, the Ser107 homologue in the human mevalonate kinase (Ser146) has been mutated to an alanine with the consequence that K_m for MgATP increased 37-fold and V_{max} decreased 4000-fold (*29*). The Ser106 and Ser107 homologues directly coordinate the tripolyphosphate chain of MgATP in the rat and *Methanococcus jannaschii* GHMP kinase structures (*10*, *25*). Together these studies demonstrate that P-loop residues are critically involved in determining both turnover and substrate recognition.

Motif III—The Substrate Recognition Loop (Serine 291 and Alanine 293). GHMP kinase active sites contain a small (five-residue) glyine-rich loop that appears well-positioned to interact with the substrate that is phosphorylated by ATP. To assess how this loop functions in catalysis, two residues of the loop (Ser291 and Ala293) were altered via mutagenesis, and the effects of the perturbations on the initial-rate parameters of the forward reaction were evaluated. Replacing the Ser291 hydroxyl with a proton (S291A) causes a 75-fold increase in $K_{i,Pmev}$ and a 19-fold increase in $K_{m,Pmev}$ compared to the wild-type enzyme. This structurally subtle, but perhaps not chemically benign, substitution significantly decreases the affinity of both the E and E·ATP forms of the

Table 2: Effects of Mutation on the Initial-Rate Parameters of the PMK-Catalyzed Reaction[a]

Conserved Element	Protein	$K_{i\ P\text{-}mev}$[b] (μM)	$K_{m\ P\text{-}mev}$ (μM)	$K_{i\ ATP}$[c] (mM)	$K_{m\ ATP}$ (mM)	k_{cat} (sec^{-1})
	Wild Type	22 (0.38) 1.0	2.4 (0.13) 1.0	2.85 (0.15) 1.0	0.31 (0.007) 1.0	18.3 (0.09) 1.0
Motif I	K9R	1130 (125) 51	130 (2.2) 54	1.8(0.027) 0.63	0.21 (0.023) 0.67	0.04 (0.0005) 0.0022
Motif II	K100A	46 (1.8) 2.1	7.3 (0.3) 3	19.75 (0.76) 7	3.1 (0.13) 10.3	11 (0.14) 0.6
	K100R	35 (0.82) 1.6	5.5 (0.27) 2.3	11.3 (0.56) 4	1.76 (0.043) 5.9	50 (0.24) 2.7
Motif III	S291A	1650 (172) 75	45 (1.0) 19	3.0 (0.074) 1.05	0.083 (0.009) 0.27	11.9 (0.083) 0.65
	S291T	31.3 (0.56) 1.5	77 (2) 32	6.3 (0.11) 2.2	15.5 (0.43) 52	4.6 (0.084) 0.25
	A293T[d]	ND[e]	42,000 (5.8) 17,500	ND[e]	4.2 (0.7) 14	0.28 (0.027) 0.015
Asp 150	D150E	39 (0.28) 1.8	2.4 (0.0085) 1.0	4.0 (0.016) 1.4	0.25 (0.0015) 0.8	1.54 (0.001) 0.084
Mobile α-Helix	S213A	29 (0.24) 1.33	9.6 (0.086) 4	8.1 (0.078) 2.84	2.6 (0.022) 8.4	3.6 (0.012) 0.196
	S213T	24 (0.42) 1.1	3.4 (0.034) 1.40	0.48 (0.006) 0.17	0.07 (0.001) 0.22	11.9 (0.033) 0.65
	Q218A	27 (0.3) 1.2	1.9 (0.1) 0.8	5.9 (0.33) 2.1	0.4 (0.006) 1.3	21.1 (0.14) 1.15
	Q218N	19.5 (0.36) 0.89	3.9 (0.064) 1.6	1.0 (0.017) 0.35	0.2 (0.004) 0.65	17 (0.1) 0.92
	K221A	16.5 (0.25) 0.75	11.7 (0.11) 4.9	0.441 (0.005) 0.154	0.313 (0.004) 1.0	15.2 (0.08) 0.83
	K221R	13 (0.17) 0.6	7.4 (0.08) 3	0.7 (0.008) 0.25	0.4 (0.0.005) 1.3	23.3 (0.12) 1.3
	Q222A	16 (0.2) 0.73	11.9 (0.16) 5	0.847 (0.01) 0.3	0.63 (0.009) 2	33 (0.25) 1.8
	Q222N	26 (0.35) 1.2	4.1 (0.08) 1.6	2.6 (0.06) 0.91	0.41 (0.006) 1.3	24.5 (0.13) 1.3

[a] A kinetic constant and its standard error are listed above the line; below it, the constant is normalized to that of the wild-type enzyme. [b] The steady-state affinity of the enzyme for Pmev in the absence of ATP. [c] The steady-state affinity of the enzyme for ATP in the absence of Pmev.[d] The kinetic constants are estimates due to the high Michaelis constants exhibited by A293T. [e] K_i values could not be determined for mutant A293T, see Materials and Methods.

Table 3: Mevalonate Inhibition of Mutant and Wild-type PMK

PMK	$K_{m,Pmev}$ (μM)	$K_{i,mevalonate}$ (μM)[a]
wild-type	2.4	126 ± 8.0
K9R	130	86 ± 11

[a] Determined from initial-rate inhibition studies, see Materials and Methods.

enzyme for phosphomevalonate during initial-rate turnover. On-the-other-hand, the substitution *enhances* the affinity of the enzyme for Mg^{2+}•ATP ($K_{m,ATP}$ decreases 3.7-fold) and, interestingly, does not effect $K_{i,ATP}$. Leaving the hydroxyl group in position and substituting the pro*R*, C_β-proton with a methyl group (S291T) has a small (1.5-fold) effect on $K_{i,Pmev}$ and causes a substantial (32-fold) increase in $K_{m,Pmev}$. Again we see that modifying this residue has a significant effect on $K_{m,ATP}$ (52-fold) and little impact on $K_{i,ATP}$. The S291A and S291T mutations have far greater effects on the steady-state ligand affinities than on turnover (k_{cat} decreases 1.5- and 4.0-fold, respectively).

The substrate synergy that occurs in the Michaelis complex is an important aspect of enzyme catalysis. These interactions, which are fundamentally allosteric, reorganize the interacting subsites and can control both the substrate affinity (which "tunes" the response of the enzyme toward metabolite concentration) and turnover. Eight angstroms separate the Ser291-hydroxyl and the closest atom of ATP (a nonbridging γ-phosphoryl oxygen). Not withstanding a significant reorganization of the active site during catalysis, it appears that the structural perturbations at Ser291 communicate at a distance (through a network of interactions) with determinants that contact and are involved in the steady-state recognition of ATP. The fact that the hydroxyl-to-proton and proton-to-methyl substitutions at the C_β of Ser291 have little or no effect on $K_{i,ATP}$ (the steady-state affinity constant for the binding of ATP to the E, as opposed to the E•Pmev, form(s) of the enzyme) reveals that the binding of Pmev at its subsite drives a structural change that is propagated to the ATP binding site, altering its affinity. While we cannot conclude with certainty that Ser291 itself participates in this Michaelis-complex synergy, it is clear is that even slight perturbations in the Ser291 structure significantly impact the allosteric network.

Alanine 293, also in the glycine-rich substrate-recognition loop, was mutagenized to threonine, and the effect of this substitution on catalysis was studied. The influence on $K_{m,Pmev}$ was profound (~17 000-fold increase), while the effect on $K_{m,ATP}$ was relatively modest (14-fold). Thus, we again see a loop perturbation selectively affecting substrate affinity with the greater effect on the affinity of the nonnucleotide substrate. Unlike the S291A mutation, the A293T substitution had a considerable effect (64-fold decrease) on k_{cat}. While it is not clear whether Ala293 itself contributes to the energetics of rate-determining steps in the catalytic cycle, it is clear that alterations at this site influence the relative energetics of the ground and transition state(s) at such steps.

Disease Correlates—The Substrate Recognition Loop. Mutating the human mevalonate kinase residue analogue of Ala293 (i.e., Ala334) to threonine causes mevalonic acid deficiency, an orphan disease that results in elevated mevalonic acid in plasma and can lead to early fatality (*30*, *31*). The recombinant, human mevalonate kinase A334T mutant exhibits a 50-fold diminution in V_{max} (*32*), which is similar to the 62-fold decrease displayed by the analogous PMK mutant, A293T. The mevalonate kinase A334T mutant also showed a significant (31-fold) decrease in its affinity for the nonnucleotide substrate. Thus, the Ala293 and Ala334 homologues exhibit similar molecular functions in these different GHMP kinases.

Position 291 is conserved across the GHMP kinase family as either serine or threonine. Mutating the Ser291 homologue in human galactokinase (T344M) causes galactokinase deficiency, which frequently results in cataract formation because the reduction of excess galactose in the lens to galactitol, by aldolase reductase, causes lens epithelial cell death (*33*). The activity of a human galactokinase T344M mutant expressed in COS cells is 10-fold lower than that of the wild-type enzyme (*5*); however, the effects on the individual initial-rate constants were not determined. The structure of the E·galactose·ADP complex of galactokinase (*Pyrococcus furiosus*) has been determined (*34*). Superposition of the galactokinase and PMK structures reveals that the positioning and structural context of the hydroxyl groups of Thr303 (the equivalent of Thr334 in the human galactokinase) and Ser291 (PMK) are virtually identical, suggesting that these two residues share a common function. Thr303 lies at the N-terminal end of a loop (motif III) that is highly conserved in the GHMP kinase family and forms part of the galactose binding pocket (*34*). To the extent that our PMK findings extrapolate across members of the GHMP kinase family, our data suggest that the molecular dysfunction associated with this particular in-born genetic error is a decrease in the steady-state affinity of galactokinase for galactose. Importantly, the present study demonstrates how information gleaned from mutagenesis of conserved residues in a representative enzyme can provide insight into the mechanism(s) of metabolic disease(s).

A k_{cat} Effector—Aspartate 150. GHMP kinase structures support that this enzyme family uses an R-group carboxylate (aspartate or glutamate) either to position lysine 9 to participate in catalysis or to coordinate the divalent cation (Mg^{2+}) associated with the tripolyphosphate chain of ATP. In PMK, this acidic residue is aspartic acid 150. To explore whether and how Asp150 might participate in catalysis, a methylene group ($-CH_2-$) was inserted into the aliphatic chain from which the carboxylate "dangles" by replacing Asp150 with glutamic acid. The effects of this R-group lengthening on the initial-rate parameters of the forward reaction are compiled in Table 2. The steady-state affinities of the substrates for various forms of the enzyme are influenced very little by the substitution (0.8−1.8-fold effects are observed); k_{cat}, however, decreases 12-fold. While the role of D150 in repositioning reactive groups at the active site is not yet certain, it is clear that lengthening the R-group primarily, if not exclusively, impacts rate-determining step-(s) in the catalytic cycle.

A Mobile Active-Site α-Helix. The binding of homoserine to the E·AMPPNP complex of the *M. jannaschii* HSK is linked to the repositioning of a conserved, active-site α-helix that completely encapsulates homoserine. To explore how regions of this helix contribute to the different steady-state functions of the enzyme, the analogous PMK helix (residues 214−221) was mutated at solvent-exposed sites along its length. Serine 213 is situated at the N-terminal end of the helix and is well conserved across the GHMP kinase EC classes (see Table 1). Threonine 183 occupies the same N-terminal position in HSK, and its hydroxyl is driven to interact with the β-phosphoryl oxygen of ATP by the binding of homoserine. When threonine is substituted for serine at position 213 of PMK, the affinity of the enzyme for nucleotide increases 5-fold with little change in the other kinetic parameters—this naturally occurring variant produces a slightly more efficient enzyme. Similar but opposing effects are observed when the serine hydroxyl is replaced with a proton by substitution with alanine: the steady-state affinity of the nucleotide decreases 8.4-fold, and k_{cat} decreases 5-fold. Thus, the N-terminal residue of the mobile helix is involved in recognition of the nucleotide and, to a lesser degree, k_{cat} and the affinity of phosphomevalonate.

Glutamine 218 is solvent-exposed and centrally positioned in the mobile helix. Neither shortening the glutamine R-group by a single methylene (i.e., Q218N) nor replacing it with alanine significantly affected catalysis. The C-terminal edge of the PMK helix contains two exposed residues, lysine 221 and glutamine 222. Conservative replacements at these sites only slightly affect initial-rate parameters; however, removing functionality by substitution with alanine at either site results in a similar pattern; the steady-state affinity of ATP for E·Pmev increases 3- to 4-fold, while the affinity of Pmev for E decreases 5-fold. Destabilization at one binding-site appears linked to stabilization at the other.

CONCLUSIONS

The 581 protein sequences and eight structures associated with the GHMP kinase family were analyzed to identify the highly conserved surface residues that are characteristic of the family. This surface-conserved set of 11 residues were mutated in a representative GHMP kinase, PMK, and the effects of mutation on the initial-rate behavior of the enzyme were studied to associate molecular functions with each member of the set. The residues were scattered across all of the motifs that define the family and exhibited functions that ranged from little or no effect on catalysis, to highly selective effects on turnover, steady-state substrate affinity, or both. Certain residues are nested within the allosteric networks that enable substrate synergy, while others affect substrate recognition without influencing synergy. What emerges from

the work is a description of the molecular functions of the conserved aspects of the GHMP kinase family that can be used in numerous of ways to understand and to control this diverse set of catalysts.

The approach described in this manuscript can be readily expanded to other protein families to create a compendium of family profiles, and it is interesting to consider the value of such a resource. The mutations contained in a database of profiles could be correlated with single nucleotide polymorphisms to establish links between disease or other phenotypes and molecular function. The information would enable biologists to study how phenotype varies as a function of well-defined changes in catalytic parameters. Genomicists and systems biologists studying metabolic flux could use the information to perturb metabolism in well-defined ways. The profiles would also provide the datasets needed to train bioinfomatic algorithms to recognize and perhaps even predict function at the residue level. These and other examples make a compelling case for the value of such a database to the biological and allied sciences.

SUPPORTING INFORMATION AVAILABLE

ClustalW alignments of GHMP kinase family sequences. This material is available free of charge via the Internet at http://pubs.acs.org.

REFERENCES

1. Bork, P., Sander, C., and Valencia, A. (1992) An ATPase domain common to prokaryotic cell cycle proteins, sugar kinases, actin, and hsp70 heat shock proteins, *Proc. Natl. Acad. Sci. U.S.A. 89*, 7290−7294.
2. Bork, P., Sander, C., and Valencia, A. (1993) Convergent evolution of similar enzymatic function on different protein folds: the hexokinase, ribokinase, and galactokinase families of sugar kinases, *Protein Sci. 2*, 31−40.
3. Luz, J. G., Hassig, C. A., Pickle, C., Godzik, A., Meyer, B. J., and Wilson, I. A. (2003) XOL-1, primary determinant of sexual fate in C. elegans, is a GHMP kinase family member and a structural prototype for a class of developmental regulators, *Genes Dev. 17*, 977−990.
4. Di Rocco, M., Caruso, U., Waterham, H. R., Picco, P., Loy, A., and Wanders, R. J. (2001) Mevalonate kinase deficiency in a child with periodic fever and without hyperimmunoglobulinaemia D, *J. Inherited Metab. Dis. 24*, 411−412.
5. Asada, M., Okano, Y., Imamura, T., Suyama, I., Hase, Y., and Isshiki, G. (1999) Molecular characterization of galactokinase deficiency in Japanese patients, *J. Hum. Genet. 44*, 377−382.
6. Zhou, T., Daugherty, M., Grishin, N. V., Osterman, A. L., and Zhang, H. (2000) Structure and mechanism of homoserine kinase: prototype for the GHMP kinase superfamily, *Struct. Fold. Des. 8*, 1247−1257.
7. Daugherty, M., Vonstein, V., Overbeek, R., and Osterman, A. (2001) Archaeal shikimate kinase, a new member of the GHMP-kinase family, *J. Bacteriol. 183*, 292−300.
8. Thoden, J. B., and Holden, H. M. (2003) Molecular structure of galactokinase, *J. Biol. Chem. 278*, 33305−33311.
9. Pilloff, D., Dabovic, K., Romanowski, M. J., Bonanno, J. B., Doherty, M., Burley, S. K., and Leyh, T. S. (2003) The kinetic mechanism of phosphomevalonate kinase, *J. Biol. Chem. 278*, 4510−4515.
10. Krishna, S. S., Zhou, T., Daugherty, M., Osterman, A., and Zhang, H. (2001) Structural basis for the catalysis and substrate specificity of homoserine kinase, *Biochemistry 40*, 10810−10818.
11. Romanowski, M. J., Bonanno, J. B., and Burley, S. K. (2002) Crystal structure of the *Streptococcus pneumoniae* phosphomevalonate kinase, a member of the GHMP kinase superfamily, *Proteins 47*, 568−571.
12. Wada, T., Kuzuyama, T., Satoh, S., Kuramitsu, S., Yokoyama, S., Unzai, S., Tame, J. R., and Park, S. Y. (2003) Crystal structure of 4-(cytidine 5′-diphospho)-2-C-methyl-D-erythritol kinase, an enzyme in the nonmevalonate pathway of isoprenoid synthesis, *J. Biol. Chem. 278*, 30022−30027.
13. Yang, D., Shipman, L. W., Roessner, C. A., Scott, A. I., and Sacchettini, J. C. (2002) Structure of the Methanococcus jannaschii mevalonate kinase, a member of the GHMP kinase superfamily, *J. Biol. Chem. 277*, 9462−9467.
14. Eisenreich, W., Schwarz, M., Cartayrade, A., Arigoni, D., Zenk, M. H., and Bacher, A. (1998) The deoxyxylulose phosphate pathway of terpenoid biosynthesis in plants and microorganisms, *Chem. Biol. 5*, R221−R233.
15. Lee, C., and O'Sullivan, W. (1985) The interaction of phosphorothioate analogues of ATP with phosphomevalonate kinase. Kinetic and 31P NMR studies, *J. Biol. Chem. 260*, 13909−13915.
16. Cleland, W. W. (1963) The kinetics of enzyme-catalyzed reactions with two or more substrates or products, *Biochim. Biophys. Acta 67*, 104−137.
17. Oberg, K. A., Ruysschaert, J. M., and Goormaghtigh, E. (2004) The optimization of protein secondary structure determination with infrared and circular dichroism spectra, *Eur. J. Biochem. 271*, 2937−2948.
18. Fasman, G. D. (1996) *Circular dichroism and the conformational analysis of biomolecules*, Plenum Press, New York.
19. McClure, W. R. (1969) A kinetic analysis of coupled enzyme assays, *Biochemistry 8*, 2782−2786.
20. Cleland, W. W. (1979) Statistical analysis of enzyme kinetic data, *Methods Enzymol. 63*, 103−138.
21. Dixon, M. (1953) The determination of enzyme inhibitor constants, *Biochem. J. 55*, 170−171.
22. Madej, T., Gibrat, J. F., and Bryant, S. H. (1995) Threading a database of protein cores, *Proteins 23*, 356−369.
23. Gibrat, J. F., Madej, T., and Bryant, S. H. (1996) Surprising similarities in structure comparison, *Curr. Opin. Struct. Biol. 6*, 377−385.
24. Bateman, A., Birney, E., Cerruti, L., Durbin, R., Etwiller, L., Eddy, S. R., Griffiths-Jones, S., Howe, K. L., Marshall, M., and Sonnhammer, E. L. L. (2002) The Pfam Protein Families Database, *Nucleic Acids Res. 30*, 276−280.
25. Fu, Z., Wang, M., Potter, D., Miziorko, H. M., and Kim, J. J. (2002) The structure of a binary complex between a mammalian mevalonate kinase and ATP: insights into the reaction mechanism and human inherited disease, *J. Biol. Chem. 277*, 18134−18142.
26. Admiraal, S. J., and Herschlag, D. (1995) Mapping the transition state for ATP hydrolysis: implications for enzymatic catalysis, *Chem. Biol. 2*, 729−739.
27. Potter, D., Wojnar, J. M., Narasimhan, C., and Miziorko, H. M. (1997) Identification and functional characterization of an active-site lysine in mevalonate kinase, *J. Biol. Chem. 272*, 5741−5746.
28. Schulz, G. E. (1992) Binding of nucleotides by proteins, *Curr. Opin. Struct. Biol. 2*, 61−67.
29. Cho, Y. K., Rios, S. E., Kim, J. J., and Miziorko, H. M. (2001) Investigation of invariant serine/threonine residues in mevalonate kinase. Tests of the functional significance of a proposed substrate binding motif and a site implicated in human inherited disease, *J. Biol. Chem. 276*, 12573−12578.
30. Hoffmann, G., Gibson, K. M., Brandt, I. K., Bader, P. I., Wappner, R. S., and Sweetman, L. (1986) Mevalonic aciduria—an inborn error of cholesterol and nonsterol isoprene biosynthesis, *N. Engl. J. Med. 314*, 1610−1614.
31. Hoffmann, G. F., Charpentier, C., Mayatepek, E., Mancini, J., Leichsenring, M., Gibson, K. M., Divry, P., Hrebicek, M., Lehnert, W., Sartor, K., et al. (1993) Clinical and biochemical phenotype in 11 patients with mevalonic aciduria, *Pediatrics 91*, 915−921.
32. Hinson, D. D., Chambliss, K. L., Hoffmann, G. F., Krisans, S., Keller, R. K., and Gibson, K. M. (1997) Identification of an active site alanine in mevalonate kinase through characterization of a novel mutation in mevalonate kinase deficiency, *J. Biol. Chem. 272*, 26756−26760.
33. Murata, M., Ohta, N., Sakurai, S., Alam, S., Tsai, J., Kador, P. F., and Sato, S. (2001) The role of aldose reductase in sugar cataract formation: aldose reductase plays a key role in lens epithelial cell death (apoptosis), *Chem.-Biol. Interact. 130−132*, 617−625.
34. Hartley, A., Glynn, S. E., Barynin, V., Baker, P. J., Sedelnikova, S. E., Verhees, C., de Geus, D., van der Oost, J., Timson, D. J., Reece, R. J., and Rice, D. W. (2004) Substrate specificity and mechanism from the structure of Pyrococcus furiosus galactokinase, *J. Mol. Biol. 337*, 387−398.

BI048963O